Spatio-temporal Stability Analysis of Linear Arrays of 2D Density Stratified Wakes and Jets

Jacob Sebastian, [1a] Benjamin Emerson,[1] J. O'Connor,[2] and Tim Lieuwen[1]

[1]*Department of Aerospace Engineering, Georgia Institute of Technology, Atlanta, GA 30332, USA*

[2]*Department of Mechanical Engineering, The Pennsylvania State University, University Park, Pennsylvania 16802, USA*

This paper investigates the spatio-temporal stability characteristics of multiple shear flow elements (wakes or jets) with density stratification. While the stability of single jets or wakes has been considered extensively, many applications exist where these canonical flow fields are aligned in multi-element configurations. A fundamental question is the relationship between the stability characteristics of a single element and the larger system. More fundamentally, this question involves the interaction of multiple regions of vorticity concentration and how they modify a system's absolute stability, as well as the manner in which density gradients influence the way these different regions of concentrated vorticity interact. This study presents a generalization of Yu and Monkewitz's [M. H. Yu, and P. A. Monkewitz, "The effect of nonuniform density on the absolute instability of two-dimensional inertial jets and wakes," Physics of Fluids A: Fluid Dynamics 2, 1175 (1990)] analysis for multiple jets and wakes, explicitly considering *n*=2, 3, 4, and infinity elements. The velocity and density base profiles are parameterized by the density ratio, *S*, velocity shear ratio, λ, and the wake spatial separation parameter, *L/D*. The results show that the maximum absolute growth rate ($\omega_{0,i}$) exhibits a non-monotonic dependence on *L/D*. In addition, the most absolutely unstable mode switches between system-sinuous and system-varicose as the spatial separation parameter is varied, in agreement with prior experiments [I. Peschard, and P. Le Gal, "Coupled wakes of cylinders," Phys Rev Lett **77**, 3122 (1996)]. This transition in symmetry, as well as the specific *L/D* value at which a given mode dominates, can be approximately predicted using the resonant wave interaction model from Juniper et al. [M. P. Juniper, "The effect of confinement on the stability of two-dimensional shear flows," J Fluid Mech 565, 171 (2006)]. Further, there are two distinct *L/D* regimes: a "near-wake regime" (*L/D*< ~3) and a "far-wake regime". In the near-wake regime, the system stability is a function of the number of elements, *n*, while in the far-wake regime, it is only the element spacing, not the number of elements that influences $\omega_{0,i}$.

[a] Author to whom correspondence should be addressed. Electronic mail: jsebastian8@gatech.edu.

I. BACKGROUND

This paper considers the spatio-temporal stability of arrays of wakes or jets. While the stability of single jets or wakes has been considered extensively, many applications exist where these canonical flow fields are aligned in multi-element configurations, either linearly, in two-dimensional arrays, or distributed azimuthally. A key question is the relationship between the stability characteristics of a single element and the larger system. More fundamentally, this question involves the interaction of multiple regions of vorticity concentration and how they modify a system's absolute stability. For example, two vorticity sheets (e.g., a jet or wake) have completely different stability characteristics than a single vorticity sheet.

This work is also motivated by the reacting shear flow problem, which is characterized by the presence of multiple, interacting shear layers and regions with large density gradients. The density gradients in the flow strongly influence the way different regions of concentrated vorticity interact. The stability of these flows plays a significant role in controlling many combustor phenomena such as mixing, entrainment, flashback and blow off [1]. In addition, they also form a feedback mechanism between the acoustics and heat release and, thus, are very important in combustion instability problems[2]. The convective/global stability of the flow, the frequency of the global mode, and the symmetry of the vortex shedding each have important influences in the behavior of the reacting flow system. The system behaves as an amplifier or self-oscillator depending on whether the system is convectively or absolutely unstable, and these stability characteristics govern the response of the system to the background acoustics. Symmetry of the vortex shedding also plays a significant role in the thermo-acoustic system characteristics. For example, Emerson et al. [3] noted that asymmetric vortex shedding causes the heat release oscillations associated with the two flames to be out of phase. This out-of-phase oscillation induces no fluctuations in unsteady heat release in the low amplitude limit, while symmetric vortex shedding causes them to be in-phase and can lead to global fluctuations in heat release. This is important as these heat release oscillations are often the source of the acoustic waves in combustion systems, acting as a key part of the overall thermoacoustic feedback loop. Emerson et al. [3] showed experimentally that, even in cases where the flow exhibited a large amplitude, sinuous global mode, that the heat release oscillations were less than those in flows with lower amplitude, varicose mode disturbances.

With this background, consider first the two-dimensional bluff body wake, which is commonly used for flame stabilization. At high Reynolds numbers, bluff body flow fields are marked by a pair of convectively unstable separating shear layers [4]. Downstream of the bluff body, these separating shear layers grow and merge in the wake. The Kelvin-Helmholtz instability leads to concentrated vortex structures in these shear layers, which interact with each other, to produce a globally unstable flow, manifested as the Von Karman vortex street [5]. Combustion alters this non-reacting flow significantly, as the density gradient from the flame modifies the interaction of one region of shear from another, as well as introduces baroclinic vorticity effects. Yu and Monkewitz[6] analyzed the stability of a density stratified wake and jet, considering flows with top-hat velocity and density profiles, parameterized by a shear ratio, $\lambda=\frac{U_b-U_u}{U_b+U_u}$, and density ratio, $S=\rho_u/\rho_b$. Here ρ_u and U_u is the reactant (un-burned) density and velocity and ρ_b and U_b is the product (burned) density and velocity. While this flow is always convectively unstable, it is only absolutely unstable for certain regions of the shear parameter and density ratio. These predicted absolute instability regions are reproduced in Figure 1, where wakes correspond to λ <0 and jets to λ >0. The figure shows that absolute instability is promoted for either wakes or jets for large absolute values of λ, i.e. for high shear rates. It also shows that high density wakes and low density jets relative to the co-flow is destabilizing. Finally, the sinuous (asymmetric) mode has the largest growth rate (and is destabilized first) for wakes, while it is the varicose mode for jets.

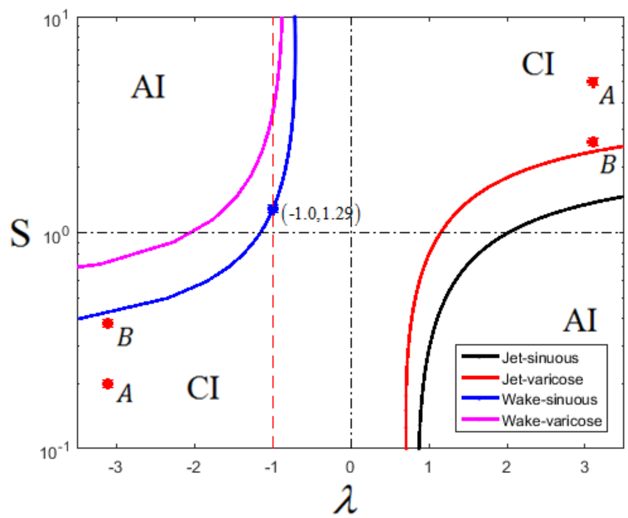

Figure 1: Predicted absolute-convective instability (AI-CI) boundary for the single unconfined wake/jet system in the *S*-λ space (following Yu and Monkewitz[6]). The points A ,B and C correspond to state of the single element in the system considered for illustrative calculations in this study. "A" corresponds to S = 0.2 and λ = -3.1 (for wake) and S = 5 and λ = +3.1 (for jet). "B" corresponds to S = 0.38 and λ = -3.1 (for wake) and S = 2.6 and λ = +3.1 (for jet). Red dashed line represents λ = -1.0 for the wake system, denoted as case C, for which the blue marker denote AI-CI boundary .

The influence of flow parameters on the dominant symmetries of flow instabilities is a common observation in many other canonical flows. For example, symmetric and asymmetric instabilities are observed for different parameter ranges for liquid jets in crossflow [7]. Similarly, Jian Deng et al. [8] explored parametric sensitivities of different flow symmetries in the wakes of airfoils. Jimenez et al. [9] explored the three-dimensional asymmetries in parallel round jets, and Ogus et al. [10] show the effects of swirl on asymmetric structures in single round jets. Likewise, Radko et al. [11] demonstrated the importance of density stratification in jets.

Returning to wakes, the analysis suggests that combustion, which leads to a lower density wake relative to the co-flow, has a stabilizing influence. This prediction has been corroborated in numerous experiments[12, 13]. For example, Emerson et al.[13] presented results from experiments that were developed in order to systematically vary the density ratio and flow velocity independently. They showed that reacting wake flows at lower density ratios, $S < \sim 0.5$, result in suppression of the narrowband velocity fluctuations in the wake that were associated with its global instability. Emerson et al.[14] also showed that the critical density ratio at which the absolute stability bifurcation occurs is very sensitive to the offset between the density and vorticity layer, due to interactions of combustion generated baroclinic vorticity and shear layer vorticity. Similarly, other studies have demonstrated the effect of density stratification on the stability of jets. For example, a canonical problem demonstrating this effect is the global instability of a helium jet emanating into a denser ambient gas, like air [15]. Sreenivasan [15] showed that absolute instability is promoted for configurations where the jet fluid is of lower density than the ambient, consistent with the theoretical predictions [6]. Ravier et al. [16] investigated the dynamics of variable density jets using direct numerical simulations and observed that the convective to absolute instability transition coincides with the appearance of global self-excited oscillations. Mario et al.[17] studied the vortex dynamics in reacting co-axial jets and identified that the presence of flame has significant influence on its flow dynamics. They observed that reacting co-axial flow can couple with the background acoustics only if forced at its natural frequency, suggesting the absolute instability character of the reacting jet system [18].

Another very relevant problem to this study of multi-element interactions is the effects of confinement on shear flow instability. Using the method of images, a confined, two-dimensional wake/jet with a confinement parameter can be shown to be equivalent to an infinite, linear array of unconfined wakes/jets with corresponding spatial separation parameter. Recent studies of the influence of confinement on the stability of wakes has shown that the instability growth rate, $\omega_{0,i}$ of the confined system (or, equivalently, of an infinite linear array of wakes/jets) is greater than or equal to the growth rate of the unconfined systems; i.e., the effect of confinement is destabilizing [19]. Theoretical investigations have shown that the destabilizing influence of confinement is a manifestation of the constructive resonant interaction of the zero group velocity modes supported by the lower velocity stream (inner flow) and higher velocity streams (outer flows) in a confined system [20] - we will return to this analysis in Sec. IV in interpreting the results of this paper.

Having provided some overview on the stability of single-element or confined wakes and jets, consider next the problem of a linear array of wakes/jets with centerline separation distance, L. A multi-element flow field can differ from that of a single-element flow in terms of steady and unsteady flow properties. For example, Zdravkovich [21] presented a comprehensive review of the two-circular wake systems in tandem, transverse and staggered configurations, showing the influence of wake-wake interactions on various mean flow characteristics. The average cylinder drag is strongly influenced by interactions. For example, the drag force of the transversely arranged system is less than twice the drag of a single cylinder system, termed “interference drag”. The interference drag increases as the cylinders are brought closer and changes rapidly (even goes to negative values) at very closer spacing[22]. The mean flow field of a wake similarly changes in the presence of an additional wake. Experiments reveals that the gap flow between the wakes tilts towards one side for small *L/D* ~1.3[23 24]. Modified mean flow causes different base pressure distribution on the cylinders [21, 25]. Thus, the close interaction of the two cylinder flows introduces lift , even though the geometric arrangement is symmetric [21, 25]. This bias in the wake structure intermittently flips, causing changes in the structure and dynamics of the flow field [26, 27]. Linear stability analysis by Carini et al. [28] suggested that a secondary instability causes the “flip-flopping” of the wake, whereas experimental work by Wang et al. [29] showed that interaction of the wake vortices from the inner shear layers of the two-body system drives the flipping.

Turning to the unsteady flow characteristics, wake separation, *L,* strongly influences both the global mode frequency and mode shape [30]. As expected, the frequency and mode shapes are nearly the same as individual flow elements for large *L/D*, typically *L/D* > 3.5[22, 26]. For smaller separations, the vortex shedding frequency of a single and two-cylinder system are different; for example, the Strouhal number of a single cylinder is *St*=0.21 for circular cylinders [31], but varies for a two cylinder system from 0.41 to 0.21 for *L/D* ranges from 1 to 3.5 [26]. Also, the 1<*L/D*<3.5 regime is characterized by the presence of two simultaneous frequencies [26,32]. In these cases, the bias in the wake flow creates one large wake and one small wake, as discussed previously. As the wake structures behind the two bodies are different, the wake shedding frequencies are also different, giving rise to vortex shedding at two different frequencies behind each of the bluff bodies. Three-bluff body flow fields also exhibit a similar variation in Strouhal number with *L/D* [26], though Sumner et al. [26] found that the range of separations over which the wake biasing is observed extends to larger *L/D*.

In addition, the global mode shape (defined by the system symmetry) also varies with *L/D*, manifested in the symmetry of the vortex shedding[22]. For two-dimensional, single wake systems, it is well known from theory that the sinuous (asymmetric) mode has a larger growth rate than the varicose mode, as shown in Figure 1. Similarly, experiments show the staggered (asymmetric) character of the von Kármán vortex street [12]. Williamson [24] presented results from flow visualization studies of the two-wake system as a function of the wake separation parameter, *L/D,* for low Reynolds numbers, $Re \approx 100$. For spacing values *L/D* < 2.0, the vortex shedding takes place in-phase, which we define later as the “system-sinuous mode” and is illustrated in Figure $5(\mathrm{a})$. However, for spacing values 2.0 < *L/D* < 5.0, the system is bi-stable, as vortex shedding intermittently flipped between anti-phase (later defined as “system-varicose mode” and shown in Figure $5(\mathrm{a})$) and in-phase (system-sinuous mode) patterns, with periods of weak and incoherent vortex shedding in between. Similarly, Peschard et al. [33] investigated the dynamics of coupled cylinder wakes. They observed system-sinuous behavior when L/D < 2.0, system-varicose behavior when L/D > 3.1, and bi-stable motion in between, which is qualitatively consistent with the earlier results. Figure 2 shows several cases corresponding to the flow patterns for the two-cylinder systems at different separation distances, which demonstrates the above-mentioned variation in flow structure with spacing. Several numerical investigations corroborate the experimental results. Mizushima et al.[34] numerically investigated the flow past a row of square bars. They observed that the flow behavior transitioned from system-sinuous to system-varicose when L/D is increased. For the most unstable mode (with the least critical Reynolds number), the transition from the system-sinuous to the system-varicose mode occur at $L/D \sim 2.7$. Kang[35], through numerical studies on two cylinder system, identified system-sinuous, system-varicose, bi-stable and biased flow patterns depending on the Re and L/D. Carini et al. [28] interpreted the bi-stable flow pattern in the two cylinder flow system as a result of the secondary instability on the system-sinuous mode, which was substantiated using the Floquet stability analysis. Thus these studies motivates the classification of the flow field as system-sinuous and system-varicose as a function of the L/D, and further explain the transition into bi-stable regime as secondary instability of the system-symmetric modes depending on the Re and L/D. Recent studies into the flow structure of the three or more bluff body wake systems also reveal similar flow regimes as in two-wake systems[26, 36-38].

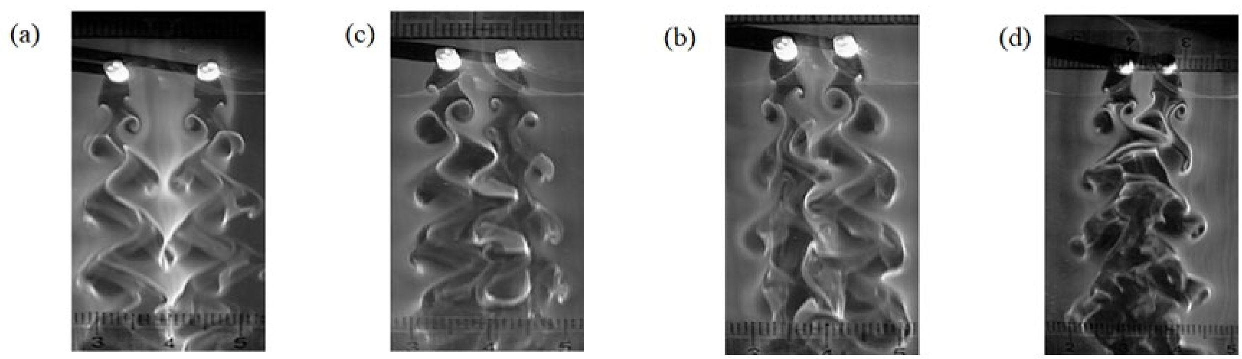

Figure 2 : Flow structure in the two-cylinder system for different separation values (a) out-of-phase flow structure (system-varicose mode), L/D = 4. (b) First asymmetric flow structure, L/D = 2.7. (c) Second asymmetric flow structure, L/D = 2.7. (d) in-phase flow structure (system-sinuous mode), L/D = 2. Symmetries of the two-wake system for the cases (a) and (d) can be compared to the system-varicose and the system-sinuous modes defined in the schematic diagram as shown in Figure 5 (a) (Reprinted with permission from I. Peschard, and P. Le Gal [33]).

Having reviewed the stability characteristics of wakes, now consider the multi-jet system. Studies show that the average jet velocities are vectored toward each other, due to lower pressure between the jets, and there is a region of recirculating flow between them [39]. The stability of multi-jet flow fields is also influenced by spacing[40]. For a large range of Reynolds numbers, single jets exhibit jet column mode oscillations at St=0.14 [41]. Experiments show a similar dominant Strouhal number for widely spaced, multi-jet systems [40, 42], but that *St* increases for smaller *L/D* [43]; e.g. Bunderson and Smith [42] show *St*~0.25 for *L/D* =1.

Analogous with the multi-wake system, the global mode structure of the multi-jet system also varies with *L/D* [40, 42]. The amplitude of the global mode for a two-jet system varies non-monotonically with *L/D*. For example, instability magnitude decreases with *L/D,* reaching a minimum at *L/D* ~7.0. It then increases with further reductions in *L/D*, reaching a maximum at *L/D* ~ 2.0. Similarly, three-jet system also exhibits large amplitude coherent structures at small *L/D* [44].

To summarize, the above review shows that the dynamics of multi-element (or confined) flow systems are significantly different from those of single element systems. Further, the observations show that the flow characteristics and structure are strong functions of the spatial separation parameter, as well as density stratification in the flow. The current work implements a local spatio-temporal stability analysis for multi-wake/jet systems, much like the spatio-temporal analyses that have been conducted for single wake systems. The results of this analysis explore the roles of the density ratio, the velocity shear ratio, the number of wakes, and the spatial separation parameter within an inviscid framework. The results provide a helpful framework for interpreting multi-element experiments, as well illustrating various general conclusions for the nature of these interactions.

II. STABILITY ANALYSIS FORMULATION

This section discusses methodology for analyzing the inviscid, linear spatio-temporal stability of a two-dimensional base flow. This is an established methodology and is widely used in the extent literature[6, 45, 46] and so is only briefly sketched out here. The flow variables – velocity components, pressure and stream function is expressed using the normal decomposition as described in equation 1. The ω and k represents the complex frequency and complex wavenumber respectively. $\hat{u}(y), \hat{v}(y), \hat{p}(y)$ and $\hat{\psi}(y)$ represents the modes for velocity components, pressure and stream function respectively.

$$\{u, v, p, \psi\}(x, y, t) = Re\{\hat{u}(y), \hat{v}(y), \hat{p}(y), \hat{\psi}(y)\}\exp\{-i\omega t + ikx\}. \tag{1}$$

Assuming the plug flow base profiles for the velocity and density (as shown in Figure 4) with no base flow velocity derivatives present, the Rayleigh equation, governing the disturbance evolution reduces to the form given in equation 2.

$$\frac{\partial^2 \hat{\psi}_1}{\partial y^2} - k^2 \hat{\psi}_1 = 0. \tag{2}$$

The general solution for the reduced form of the Rayleigh equation is given as in equation 3.

$$\hat{\psi}_1(y) = A\exp(ky) + B\exp(-ky). \tag{3}$$

Matching conditions at the interfaces specify the jump in the flow variables. Equation 4 describes the kinematic matching condition across the interface, in which the $\hat{\psi}_i$ and U_i describe the flow quantities in the respective domains.

$$\Delta\left[\frac{\hat{\psi}_i}{(U_i - c)}\right] = 0. \tag{4}$$

Similarly, the equation 5 dictates the pressure matching condition at the interface.

$$\Delta\left[\rho_i \hat{\psi}_i (U_i - c) - \rho_i \hat{\psi}_i U_i'\right] = 0. \tag{5}$$

Matching conditions at the interface yield the dispersion relation, which relates the complex ω and k. Further, the modes with zero group velocity, $\left(\frac{\partial\omega}{\partial k}\right) = 0$, manifested as saddle points in the complex wavenumber plane is identified. The saddle points which satisfy the Briggs-Bers criteria are the valid saddle points which contribute towards absolute instability [47]. Figure 3 shows the contours of the in the complex wavenumber plane showing the dominant saddle for a reference case of λ=-2.0 and S=1.0. The growth rate of the valid zero group velocity mode with the maximum growth rate gives the $\omega_{0,i}$ of the system. Positive growth rate of the zero-group velocity mode implies that the mode is absolutely instable mode, whereas the negative growth rate corresponds to a convectively unstable mode. This stability analysis framework is used to reproduce the results in Yu & Monkewitz [6] and is shown in Figure 1.

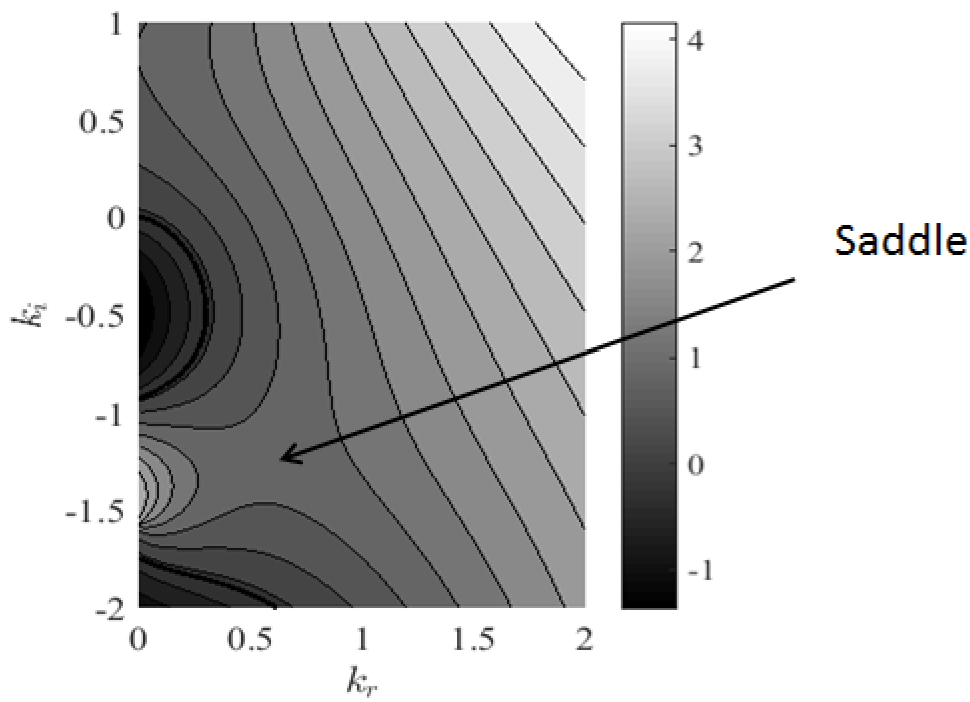

Figure 3: Contours of ω in the complex k plane for unconfined sinuous wake with $\boldsymbol{\lambda}$=-2.0 and S=1.0

This work generalizes the profiles considered by Yu and Monkewitz[6] to multiple wakes/jets, with n = 2, 3 and 4, in order to directly compare these results to those obtained from their analysis. Figure 4 shows the base flow velocity and the density profiles used to model the multi-wake/jet problems, using the two-wake and three-wake systems as examples. Each bluff body wake is represented by discontinuous plug flow velocity and density profiles. The base flow parameters are the density ratio (S), the velocity shear ratio (λ), the spatial separation parameter (L/D), and the number of wakes/jets (n). Equations 6 and 7 define the velocity shear ratio and the density shear ratio, respectively. By imposing boundary conditions simulating confinement, the n-jet/wake system can also be generalized to study the stability of an infinite linear array of jets/wakes with n-fold symmetry.

Similar to the work of Yu and Monkewitz, this paper uses the Rayleigh equation to model the multi-wake problem in an inviscid framework. Thus, this work is relevant to high Reynolds number flows. More generally, viscous effects influence the flow structure at lower Reynolds numbers. For example, single wakes undergo a global stability bifurcation at a critical Reynolds number near Re_c=46 [48, 49], as well as a series of other bifurcations associated with shear layer and wake structures with increasing Reynolds number[48, 49].

It is helpful to also consider problems with imposed sinuous or varicose symmetry on perturbations at the centerline, to isolate the stability of modes with that imposed symmetry. This is identical to simulating the full domain (and produces the same modes), but calculations that independently target these two modes facilitate tracking and continuation during parametric sweeps. This symmetry (defined as system-sinuous and system-varicose) represents the symmetry of the entire multi-wake system, as well as the symmetry of the central wake for systems with odd numbers of wakes.

$$\lambda = \frac{U_{inner} - U_{outer}}{U_{inner} + U_{outer}}, \tag{6}$$

$$S = \frac{\rho_{inner}}{\rho_{outer}}. \tag{7}$$

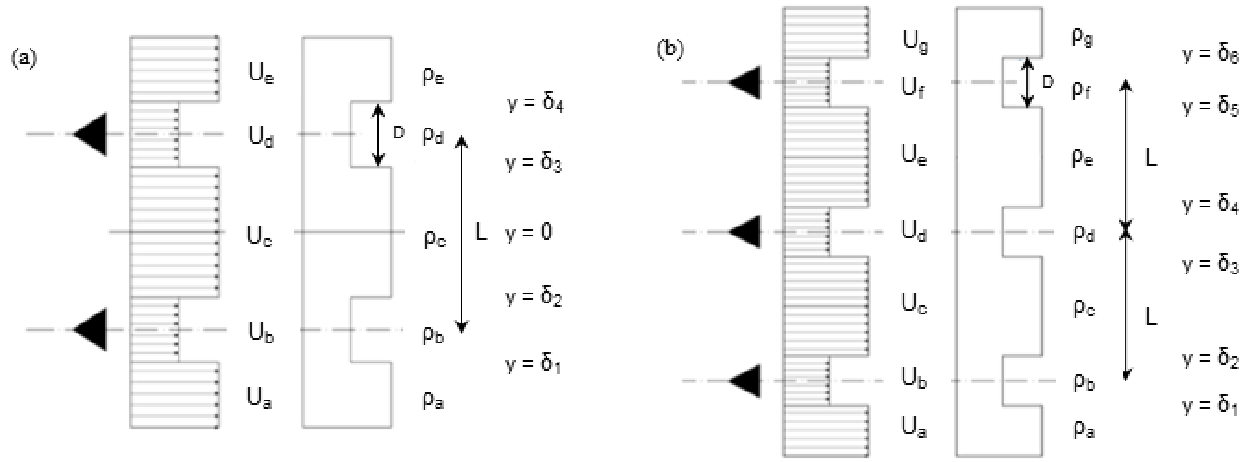

Figure 4: Base flow velocity and density profiles for a) the two-wake system and b) the three-wake system

For the base flow profile shown in Figure 4, outer velocity is defined to be, $U_{outer} = U_a = U_c = U_e$. At the same time, the inner velocity is defined to be $U_{inner} = U_b = U_d$. Similarly, the inner (ρ_{inner}) and outer density (ρ_{outer}) is also defined. A spatio-temporal stability analysis on these base flows computes the $\omega_{0,i}$ of the system and its system-sinuous and system-varicose counterparts. For the unconfined single jet/wake system, Yu and Monkewitz[6] derived the following dispersion relation for this system,

$$S\frac{(1+\lambda-c)^2}{(1-\lambda-c)^2} = -\frac{e^k + se^{-k}}{e^k - se^{-k}}, \tag{8}$$

$$s = \begin{cases} +1 : sinuous\ mode \\ -1 : varicose\ mode \end{cases} \tag{9}$$

where c denotes the disturbance phase speed, $c = \omega / k$.

Yu and Monkewitz[6] further noted that these equations remain invariant in the transformation, $S \leftrightarrow S^{-1}; \lambda \leftrightarrow -\lambda; s \leftrightarrow -s$. This reveals that the wake solution with sinuous symmetry is equivalent to the jet solution with varicose symmetry, with density ratio inverse that of the wake and vice versa. This result can be seen in Figure 1. Using a similar transformation, the multi-wake transformation maps onto multi-jet results, as will be discussed in the next section.

For reasons discussed in the introduction, the symmetry of the most rapidly growing modes is of great interest. Multiple symmetries can be defined, based upon the symmetry of a given element with respect to its centerline, as well as that of the system. The symmetry of the modes is quantified across the center of the system and across the individual element using the following system-varicose and system-sinuous decomposition of the pressure field [3].

$$p(x, y, z) = p_s(x, y, t) + p_v(x, y, t), \tag{10}$$

$$p_s(x,y,z) = \frac{p(x,y,t) - p(x,-y,t)}{2}, \tag{11}$$

$$p_v(x,y,z) = \frac{p(x,y,t) + p(x,-y,t)}{2}. \tag{12}$$

In these equations, $p_s(x,y,z)$ and $p_v(x,y,z)$ correspond to the sinuous and varicose decomposition of the pressure field respectively. To illustrate the idea for a two element system, the symmetry of the flow field is defined for the individual wakes ($\hat{S}_{wake}$, defined with respect to the center of the wake) as well as for the overall system ($\hat{S}_{system}$) based on the fraction of the sinuous component of the pressure field in the total pressure field.

$$\hat{S}_{system} = \left[\frac{p_{s,rms}}{p_{s,rms} + p_{v,rms}} \right]_{y=-L}^{y=+L}, \tag{13}$$

$$\hat{S}_{wake} = \left[\frac{p_{s,rms}}{p_{s,rms} + p_{v,rms}} \right]_{y=-D}^{y=+D}. \tag{14}$$

We will utilize the following terminology to differentiate between these different symmetries. We define the multi-wake system as having 'system-sinuous' behavior when the system symmetry across its center is sinuous. Alternatively, the system shows 'system-varicose' behavior when the system symmetry is varicose. Analogously, let "wake-sinuous" and "wake-varicose" define the modes with sinuous and varicose symmetry across the center of the individual wakes respectively. To help visualize the interplay between wake symmetry and system symmetry, Figure 5 (a) and (b) illustrates the potential combinations of symmetries of the overall flow and the individual wakes for the n=2 and 3 systems, respectively. Considering Figure 5 (a) and (b), it shows that a single individual wake may exhibit either varicose or sinuous motions (represented by Figure 5-(ii) & (iv) and Figure 5-(i) & (iii) respectively), and that the $n=2$ and 3 systems may exhibit system-varicose or system-sinuous motions (represented by Figure 5(iii) & (iv) and Figure 5(i) & (ii) respectively). Similarly, we can also decompose the flow field into sinuous and varicose components across the wake interfaces as well. For example, for $n=3$ system, Figure 5(b)-(ii) & (iv) shows the shear layer arrangement with varicose symmetry and Figure 5(b)-(i) & (iii) a sinuous symmetry across the interface. Note that for $n=2$ system, the interface symmetry is the same as the system symmetry.

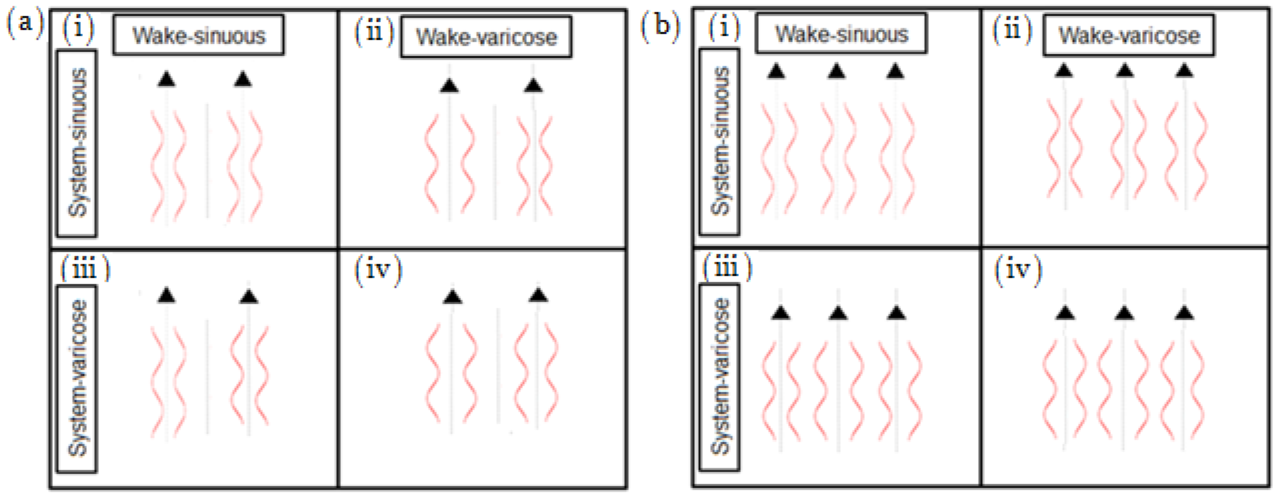

Figure 5: Different symmetries across the center of the multi-wake system and across individual wakes of the (a) two-wake system and (b) three-wake system.

In addition to finite-wake systems, we also model an infinite wake system. The $n=\infty$ wake system has an infinite number of possible symmetries of the individual wakes, and an infinite number of possible symmetries of the wake-wake interfaces. Some of the possible symmetries of the $n=\infty$ system can be modeled as confined wake systems using method of images. Therefore, to model the infinite wake system as a confined wake system requires knowledge of the most amplified symmetries. To address this, we observe the symmetries that tend to be most amplified with finite numbers of wakes. As shown later in the Results section, these symmetries typically consist of simple patterns: sinuous wakes that are separated with either a sinuous or a varicose condition. Therefore, we model the infinite wake system with two models: a single confined wake with sinuous boundaries, and a single confined wake with varicose boundaries.

III. RESULTS

Section II above detailed a spatio temporal stability analysis for the multi-wake system of identical elements as a function of four parameters: density ratio, S, shear ratio, λ, spatial separation parameter, L/D, the number of wakes, n, as well as whether or not some symmetry is imposed at the centerline. Figure 1 provides useful context for understanding the results, as it plots the absolute-convective stability boundaries of individual elements. We next consider three case studies whose S-λ values are denoted on Figure 1 as case A: (S = 0.2 and λ = -3.1), case B (S = 0.38 and λ = -3.1), and case C (λ = -1). Note that cases A and B both correspond to cases that are absolutely stable, with case B lying closer to the stability boundary than case A. Case C is not a single condition but a sweep over S values at fixed λ = -1; at this condition, the critical S value (which correspond to the AI-CI boundary) varies much more rapidly with λ than in cases A and B.

Figure 6(a) and Figure 6(b) plots the dependence of the $\omega_{0,i}$ for the general two wake system, along with the $\omega_{0,i}$ of the system-sinuous and system-varicose two wake system, as a function of *L/D* for cases A and B. Here, the general two wake system is solved for two neighboring wakes (see Figure 4a)). The systems with imposed symmetries (system-sinuous or system-varicose), are solved as a single wake with a symmetry boundary condition (sinuous or varicose) to model the second wake by method of images (see Figure 5a). Two reference lines are also indicated, corresponding to the $\omega_{0,i}$ of a single wake with width *D* and 2*D*. The former and latter cases describe the two limiting cases – the single wake result capturing the $L/D \to \infty$ case, where interaction effects become negligible, and the 2*D* wake width capturing the limit where the wakes merge into a single wake, which is the *L/D* =1 case. More generally, for an *n*-wake system, the multi-wake collapses onto a single wake with equivalent diameter of *nD* at *L/D*=1. Figure illustrates that the two-wake system retract back to the respective single wake behavior- single wake with a diameter=*2D* as $L/D \to 1$ and single wake with diameter=*D* as $L/D \to \infty$, in the asymptotic limits of the *L/D*.

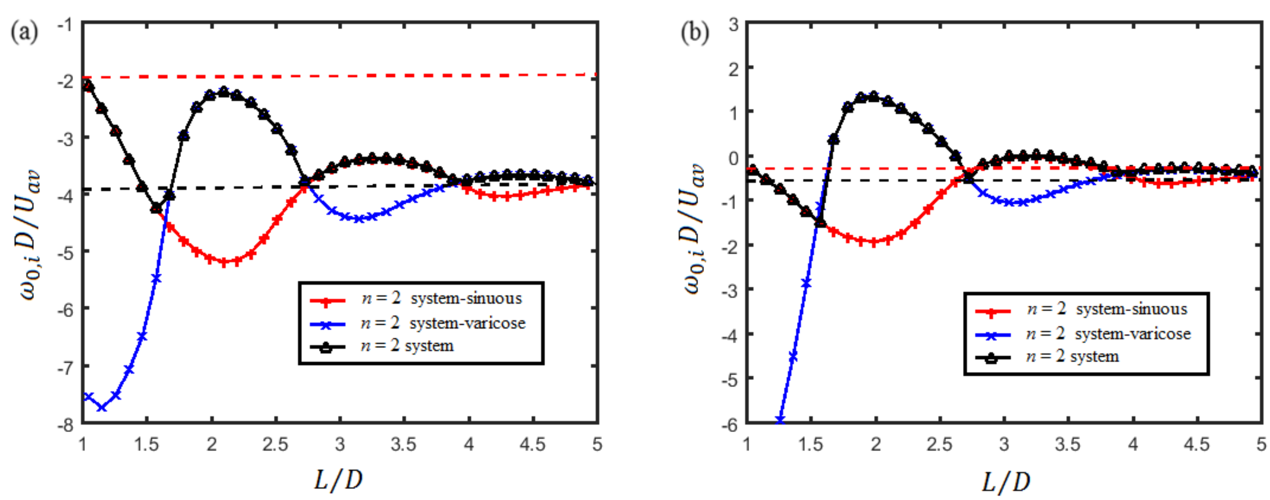

Figure 6: Dependence of normalized $\omega_{0,i}$ of two-wake system, along with that of imposed system-sinuous and system-varicose symmetry systems, upon *L/D* for the cases (a) case A and (b) case B. Black and red dashed lines represent the unconfined single wake with diameter *D* and *2D* respectively.

Further, the figure illustrates several important results. First, the $\omega_{0,i}$ of the system varies non-monotonically with *L/D*. Similarly, the growth rate of the system-sinuous and system-varicose cases also varies in a non-monotonic manner with *L/D*, with alternating regions of dominance between them with *L/D*. For example, the system-varicose mode has a larger growth rate than the system-sinuous for 1.5<*L/D*<2.7, 3.9<*L/D*<5.0, and so forth. Second, the $\omega_{0,i}$ of the two-wake system follows $\omega_{0,i}$ of the system-sinuous or system-varicose mode, depending on whichever is dominant. These results implies that the overall symmetry of the unsteady motions change with *L/D*, exactly what was seen in the experiments reviewed in the introduction and shown in Figure 2. We will return to this point in further detail in the section IV.B.

Third, comparison of the two-wake results with the unconfined single wake shows that the presence of additional element have a destabilizing influence on the system. For example, case B, which is nearly absolutely stable for an unconfined single element, becomes absolutely unstable for 1.6<*L/D*<5.0.

Next, consider the manner in which the location of the stability boundary in *S* - *L/D* space changes with *L/D*. For this purpose, Figure 7 shows the absolute-convective instability boundary as a function of *S* and *L/D* for case C. The changes in stability boundary are larger for case C than case A and B, as can be anticipated from Figure 1. The dominance of different system-sinuous and system-varicose modes at different regimes of the spatial separation, *L/D*, results in the switching of the symmetry of the flow structure. Further, the two-wake system converges to its single wake counterpart in the $L/D \rightarrow \infty$ limit, as expected. These theoretical results are compared with that of the variation of the flow patterns observed in the prior experimental and numerical studies in section IV.B.

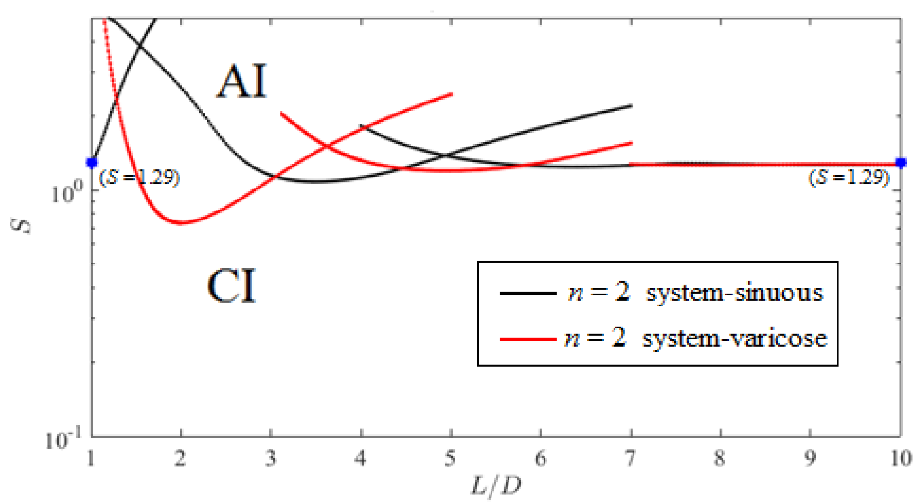

Figure 7: Dependence of absolute-convective instability boundary on *L/D* for the two-wake system as a function of *S*- *L/D* for case C. The black and red curves correspond to the system-sinuous modes and system-varicose modes respectively. Blue marks represents the unconfined single wake stability boundary for case C[6], as shown in Figure 1.

Now consider the three wake system. The base flow profile of any odd-*n* value system has a key difference compared with an even-*n* value system, in that the former has an element at the center of the system, while the latter does not. This leads the three wake system (or generally any odd *n*-value system) to exhibit a system-sinuous mode, since the center wake has sinuous mode as the most absolutely unstable mode. Figure 8 shows the absolute stability characteristics of the three-wake system as a function of *L/D* for cases A and B, with reference lines representing the unconfined single wake results with diameter *D* and *3D*.

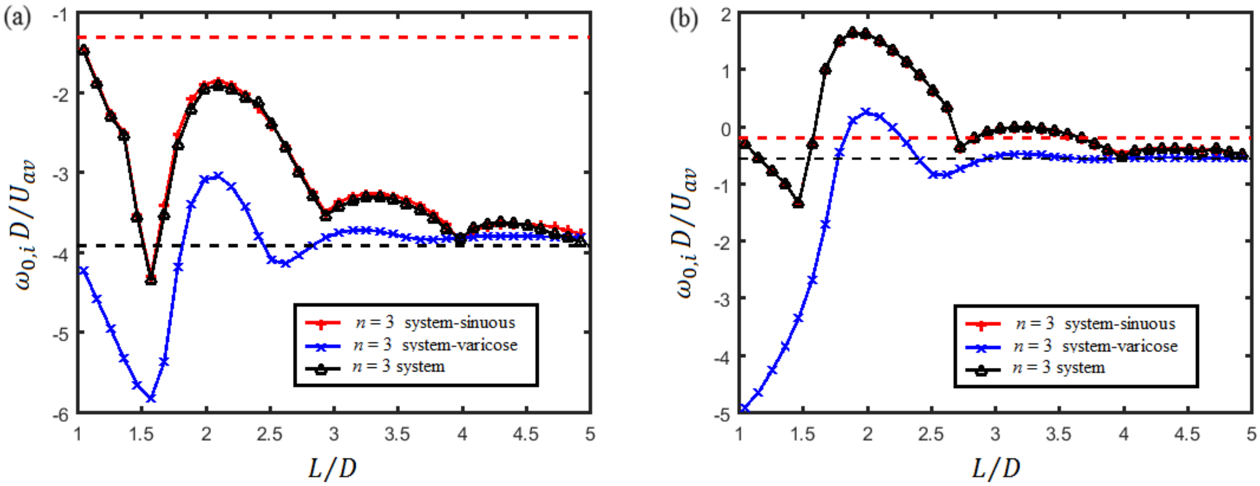

Figure 8: Dependence of normalized $\omega_{0,i}$ of the three-wake system, along with that of system-sinuous and system-varicose symmetry systems, upon L/D for the cases (a) case A and (b) case B. Black and red dashed lines represent the unconfined single wake with diameter D and $3D$ respectively.

The figure reveals some important spatio-temporal stability characteristics of the three wake system. First, the three wake system converges into an unconfined single wake with diameter = 3*D* at *L/D* = 1, whereas the system behaves as an unconfined single wake with diameter = *D* at large *L/D*. Second, the $\omega_{0,i}$ of the system varies non-monotonically with *L/D*, similar to the two-wake counterpart. However, in contrast to the two wake system, the most dominant mode for the three wake shows system-sinuous behavior for whole range of *L/D*. Further, the comparison of the three-wake $\omega_{0,i}$ with the unconfined single wake results (corresponding to the large *L/D* limit) demonstrates the generally destabilizing influence of the additional element, except for a small region of ~1.4<*L/D*<1.6 for case A and ~1.1<*L/D*<1.6 for case B.

Consider next the four-wake, *n*=4, system. As in the two-wake system, the dominant mode of the four-wake system can be either system-sinuous or system-varicose, as defined in the previous section, by virtue of it's profile geometry. Figure 9 shows the comparison between the spatio-temporal characteristics of two-, three-, and four-wake systems as functions of *L/D* for the two *S*-λ cases, case A and case B, considered. In addition, the solid lines show the stability characteristics of the confined single wake (with imposed sinuous and varicose wall boundary conditions), which is equivalent to $n=\infty$ systems with respective symmetry at the interface (care was taken to neglect the ambiguous instability modes[20]). Several observations can be deduced from this result. First, all the multi-wake systems, as well the confined wake system, limit to the behavior of the single wake system in the limit of the high *L/D*. Similarly, the multi-wake system limits to the behavior of the single wake system with *nD* diameter, in the limit *L/D*=1. Second, we can characterize two distinct regimes of *L/D*: a "near-wake" regime (*L/D*< ~3) and a far-wake regime (*L/D*> ~3). In the near-wake regime, the stability characteristics of the *n*= 2, 3, and 4 systems differ from each other, as well as depending upon *L/D*. In the far-wake regime, they progressively collapse onto a single curve that varies with *L/D.* In other words, in the near-wake regime, the number of elements influences the overall system stability, while in the far-wake regime, it is only the *element spacing*, not the *number of elements* that influences the $\omega_{0,i}$. Third, except for values near *L/D* ~ 1 (*L/D* ~1.0<*L/D*<1.2 for case A and *L/D* ~1.0<*L/D*<1.5 for case B), the $\omega_{0,i}$ of the multi-wake system progressively converges toward the confined wake system (which models an infinite wake system) in both the near-wake and far-wake regime, as the number of wakes are increased. Note that as *L/D* →1, the multi-wake system has two relevant length scales; a single wake of width *nD*, and a sequence of *n*-1 jets of width *L-D*. In contrast, the confined wake system has only the jet length scale, *L-D*. This results in the $\omega_{0,i}$ of the multi-wake system deviating from that of the confined wake system in the limit of *L/D*=1. Similarly, the *L/D* values at which the mode switches from system-sinuous to system-varicose converges to the corresponding result from the confined (infinite) wake system, as the number of wakes increases. Thus, this demonstrates that symmetry at the wake-wake interface switches from sinuous to varicose with variation in *L/D*.

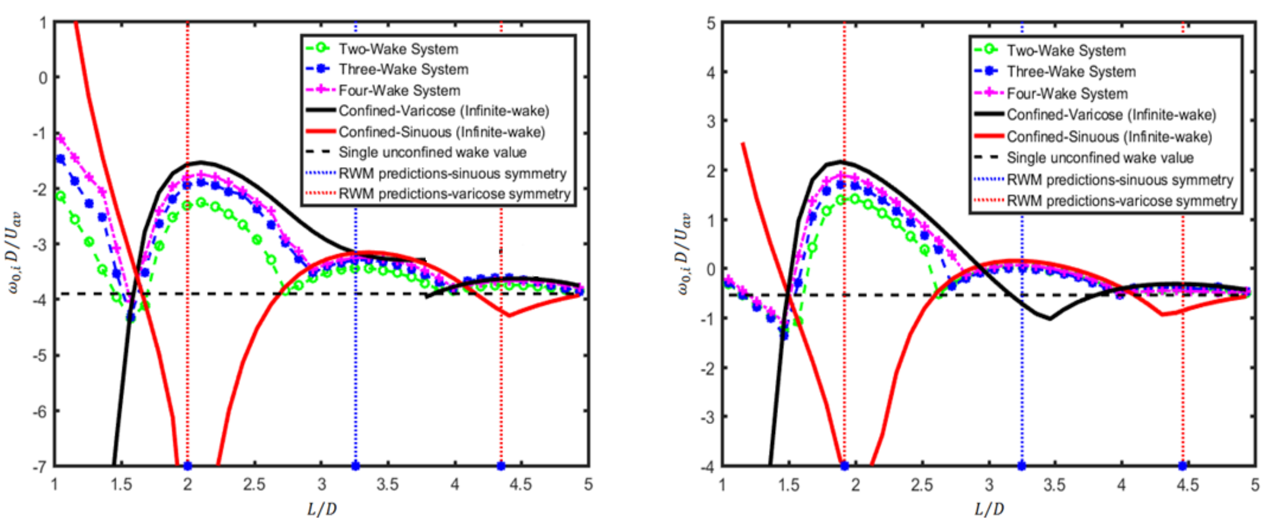

Figure 9: Comparison between the stability characteristics of the multi-wake systems and confined wake system (representing the infinite wake system). Plot shows non dimensionalised $\omega_{0,i}$ as function of *L/D* for the a) case A and b) case B. Black dashed line represents the unconfined single wake with diameter *D*. Red dashed lines and associated blue marks denote the critical *L/D* discussed in Section A

This equivalence of the infinite-wake system to the confined wake system follows that the most absolutely unstable mode favor a sinuous/varicose symmetry across the wake interface. To demonstrate this point, let us analyse the mode shape for a *n*= 3 system as a function of *L/D*. Figure 10(a) and (b) shows pressure mode shapes of the *n*= 3 system for *L/D* = 1.36 and *L/D* = 2.0 respectively. The comparison of the pressure mode shapes at two *L/D's* reveals some important points. First, both the cases, with *L/D* = 1.36 and *L/D* = 2.0, exhibit system-sinuous symmetry. As noted earlier, a *n*= 3system always exhibits system-sinuous behavior. Second, symmetry across the wake-wake interface is different for the two cases. For $n=3$ system with L/D=1.36, the symmetry of the mode is sinuous at the wake-wake interface, which can be correlated to Figure 5(b)-(i). In contrast, the system has varicose interface symmetry for the case with L/D=2.0, and can be compared with Figure 5(b)-(ii). Thus, this demonstrates that symmetry at the wake-wake interface switches from sinuous to varicose with variation in L/D.

The behavior of the n=even multi-element system, represented by the symmetry of the dominant mode shape, transition from system-sinuous to system-varicose with variation in L/D. For reasons discussed in Section A the transition L/D value at which the dominant mode transitions between system-sinuous and system-varicose varies with S and λ for the even-n wake system. To illustrate, Figure 11 plots the AI-CI stability boundary in the λ - L/D parametric space for the two-wake system for density ratios of S=1.5, S=1.0 and S=0.75. The plot delineates the regions where the system-sinuous and system-varicose mode dominates for each of the three cases. Absolute instability is suppressed with decrease in density ratio, as discussed in the introduction. In addition, the density ratio influences the transition L/D value at which the system transition from system-sinuous to system-varicose symmetry. For example, the transition L/D value for the S=0.75 and 1.5 case changes from 1.5 to 1.35 for the first transition, from 2.8 to 3.2 for the second, and from 4.1 to 4.6 for the third. Similar comments hold for the shear ratio.

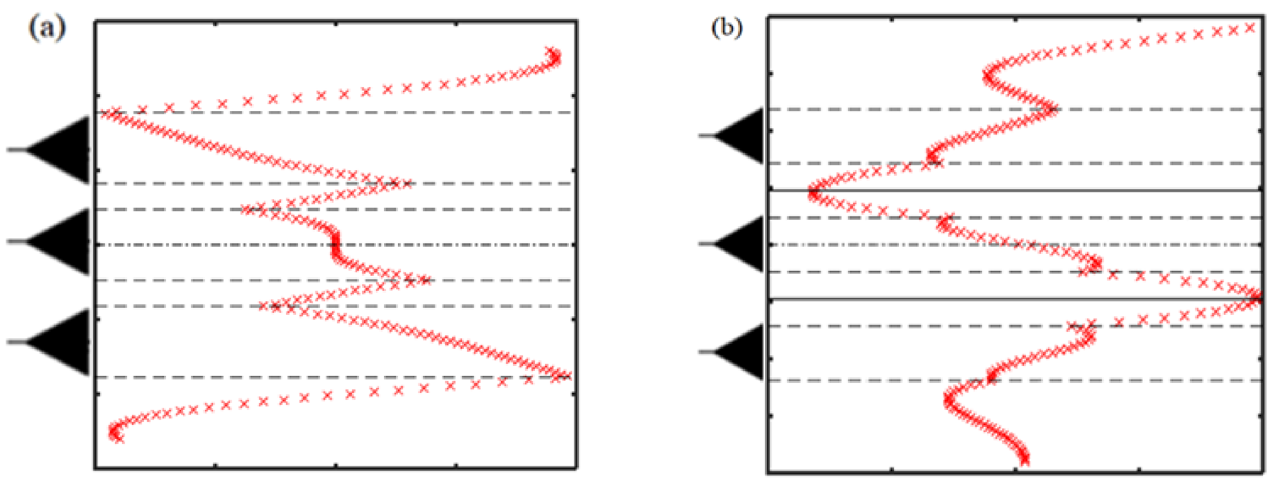

Figure 10: Pressure mode (spatial distribution of the pressure) for the three-wake system for the case S = 0.2 and λ = -3.1 for a) L/D = 1.36 and b) L/D = 2.0

As discussed previously, Yu and Monkewitz[6] demonstrated symmetry in the dispersion relations of single wakes and jets. Thus, the dispersion relation for a confined wake system is invariant under the transformation, $S \leftrightarrow S^{-1}; \lambda \leftrightarrow -\lambda;$ and sinuous wall BC transformed to varicose wall BC. Likewise, the infinite wake system has an equivalent infinite jet system since it is equivalent to the confined wake system. Finite multi-element systems also follow this tranformation. For example, a two-wake system with system-sinuous symmetry is equivalent to a two-jet system with system-varicose symmetry, with each individual wake transformed by $S \leftrightarrow S^{-1}; \lambda \leftrightarrow -\lambda;$.

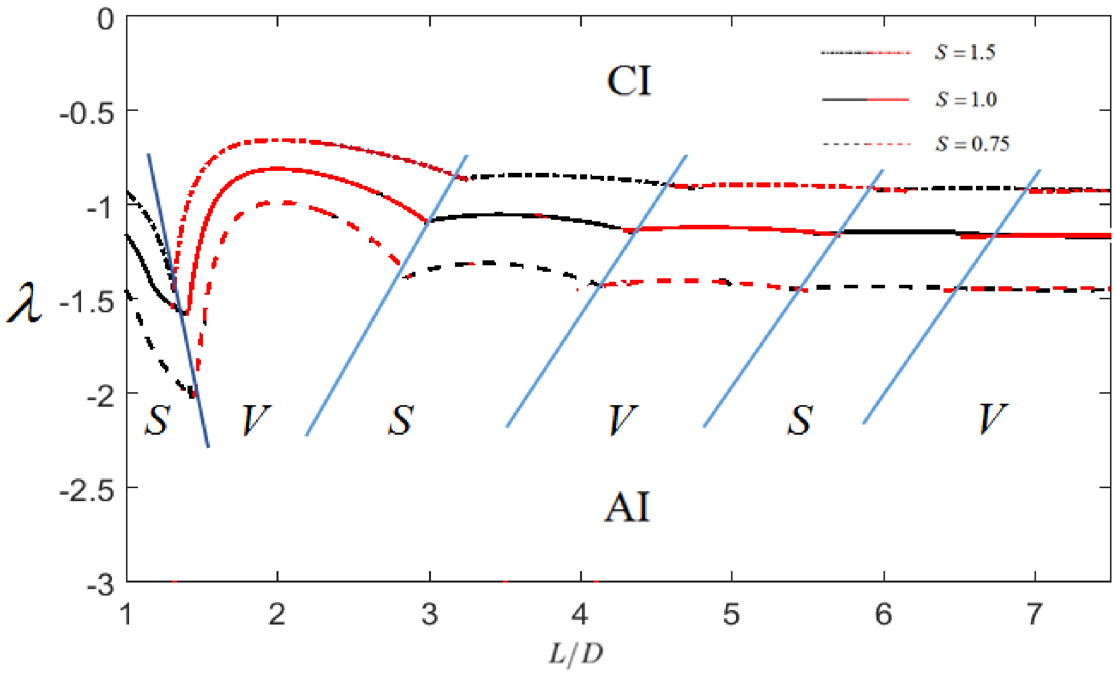

Figure 11: Dependence of the AI-CI stability boundary of the two-wake system in the λ - *L/D* parametric space for different density ratios. The region beneath the curve represent the AI regime and vice versa. S and V regimes of *L/D* represent the system-sinuous mode and system-varicose mode regimes of *L/D* respectively.

To conclude, the number of wakes and their spatial separation influence the spatio-temporal stability characteristics of multi-wake systems. First, stability behavior of the multi-wake system varies non-monotonically with *L/D*. All multi-wake systems converge to the same behavior for large and small *L/D* limits. As *L/D* →1, they converge to the behavior of the corresponding single wake system with a diameter equal to *nD* (the merged wake diameter, i.e. the sum of the diameters of all of the wakes). As *L/D* $\rightarrow \infty$, the system converges to the behavior of the single wake system with the diameter of a single wake. In this limit, the wakes are independent and do not interact. Further, we can characterize two distinct regimes of *L/D*: a "near-wake regime" (*L/D< ~3.0*) and a "far-wake regime" (*L/D> ~3.0*). In the near-wake regime, the stability characteristics of the *n*= 2, 3, and 4 systems are different from each other. In the far-wake regime, they asymptote to the same $\omega_{0,i}$. Thus, in the near-wake regime, adding additional elements changes the overall system stability, while in the far-wake regime, it is only the element spacing, not the number of elements that influences the $\omega_{0,i}$. Second, the symmetry across the center of the system for the most unstable mode vary with *L/D*. A system with *n*=even favors both system-sinuous and system-varicose modes which alternate with increasing *L/D.* In contrast, *n*=odd wake system exhibit system-sinuous mode by virtue of it's base flow profile.

IV. DISCUSSION

This section is divided into two subsections. In the first subsection, we discuss the application of a resonant wave interaction model (RWM) to explain the spatio-temporal stability behavior of multi-wake systems. As will be shown, this RWM model closely predicts the *L/D* values corresponding to maximum values of the $\omega_{0,i}$. Then, the next sub-section discusses the stability analysis results in the context of the previous investigations on multi-wake systems.

A. Resonant Wave Interaction Model (RWM)

This section presents a model to explain the preferential amplification of the system-varicose/sinuous modes for different ranges of *L/D*. It also provides a framework to model the specific values of *L*/*D* where the wake mode of maximum $\omega_{0,i}$ switches between system-sinuous and system-varicose structure. This work closely follows Juniper et al.[20], who showed that for a confined wake system, the confinement that delivers maximum $\omega_{0,i}$ is the one where "resonant interaction" occurs. Thus, the RWM offers an approach to predict the *L/D* values associated with local maxima of the $\omega_{0,i}$.

The framework for the RWM is a confined wake with imposed symmetry (sinuous or varicose) of the confining walls [20, 49, 50]. Figure 12 schematically shows the confined wake and its two nearest images, as well as defining an "inner flow" and an "outer flow" within this framework of images. The inner flow is defined as the central wake feature (a velocity deficit and its neighboring, faster base flow regions). The outer flow is defined as a jet that is composed of the faster base flow region, surrounded on one side by the central velocity deficit and on the other side by an image of the velocity deficit. The resonant interaction model separately calculates the $\omega_{0,i}$ of these inner and outer base flow regions, by assuming weak and strong confinement respectively. A resonant condition is defined as one where the inner and outer flows have equal absolute wave numbers, k_0 (i.e., the zero group velocity mode or its subharmonics in each of these flows have the same wave number). Two situations are modeled: one with a sinuous wall boundary condition, and one with a varicose wall boundary condition. Juniper et al.[20] showed that the $\omega_{0,i}$ peaks (i.e., has a local maximum) at confinement or *L/D* values where that model (sinuous or varicose) has matching values of k_0 for the inner and outer flows.

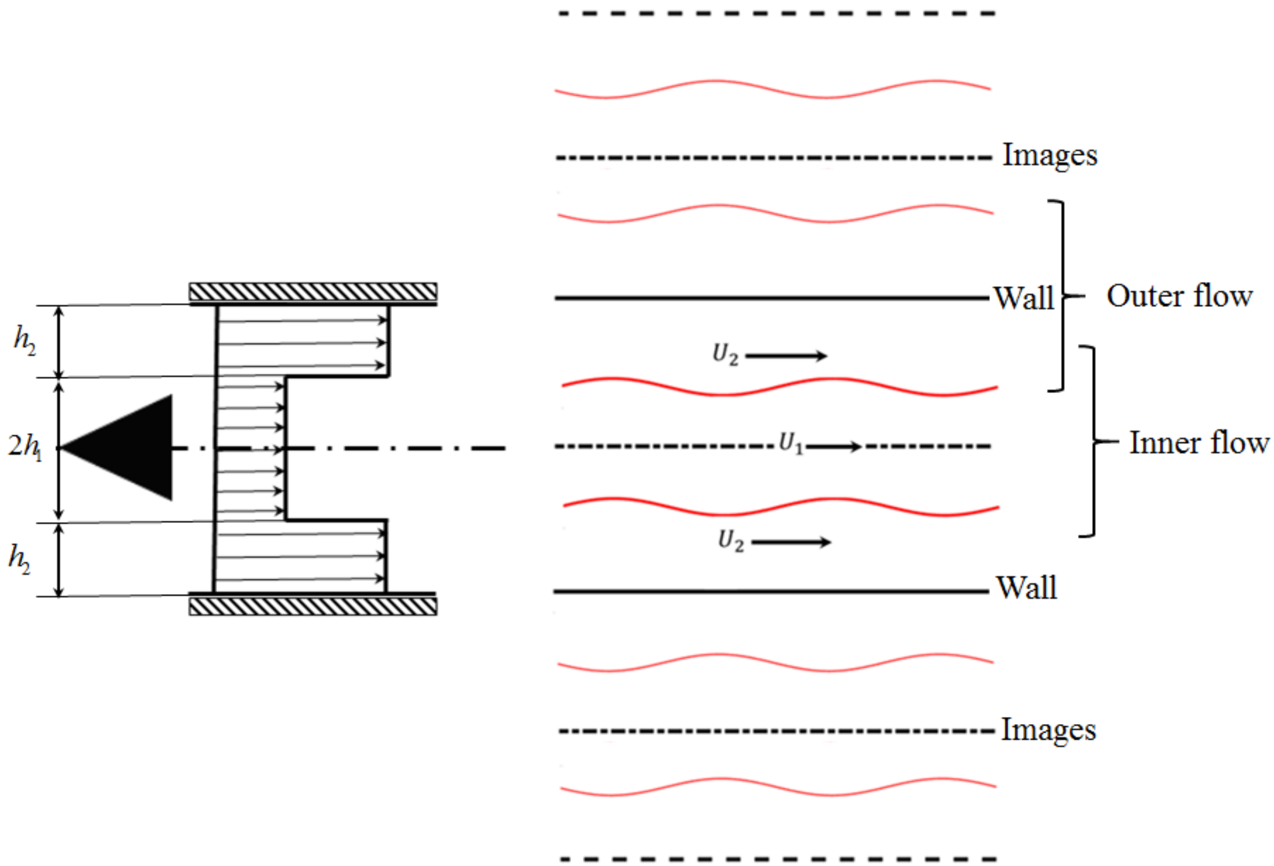

Figure 12. Confined wake system represented using the method of images, illustrating the inner and outer flow regions

The RWM is best suited for intermediate values of confinement, where the inner and outer flow regions interact. In contrast, the limits of weak and strong confinement (i.e. $L/D \rightarrow \infty$ and $L/D \rightarrow 1$, respectively) correspond to the dominance of the inner flow and outer flow regions, respectively. In other words, under strong confinement, the shear layers of the outer flow are more closely spaced than the shear layers of the inner flow, as depicted in Figure 13, and consequently interact strongly. In this case, the outer flow has higher $\omega_{0,i}$. In contrast, weak confinement moves the inner flow's shear layers close together so that they control the maximum absolute growth. Thus, flows with weak confinement (large L/D) will tend to have a dominant instability mode that resembles a single unconfined wake, which manifests as a cascade of independent sinuous features. Flows with strong confinement (small L/D) will tend to have a dominant instability mode that resembles a single unconfined jet- they will exhibit a cascade of independent varicose features.

The approach is best illustrated with an example using case A. First, the model is constructed with varicose wall boundary conditions as illustrated in Figure 13. This configuration models the dynamics of an $n = \infty$ system where the dynamics of each wake are partitioned from the neighboring wakes' dynamics with varicose symmetry. In the case of strong confinement this system would be dominated by the outer flow (illustrated in Figure 13) with characteristic length scale of h_2, which is proportional to the wake spacing. Similarly, the weak confinement case is dominated by the inner flow with characteristic length scale h_1, which is proportional to the wake width. These lengths scales are related to the wake separation parameter as, $L/D = 1 + h_2/h_1$.

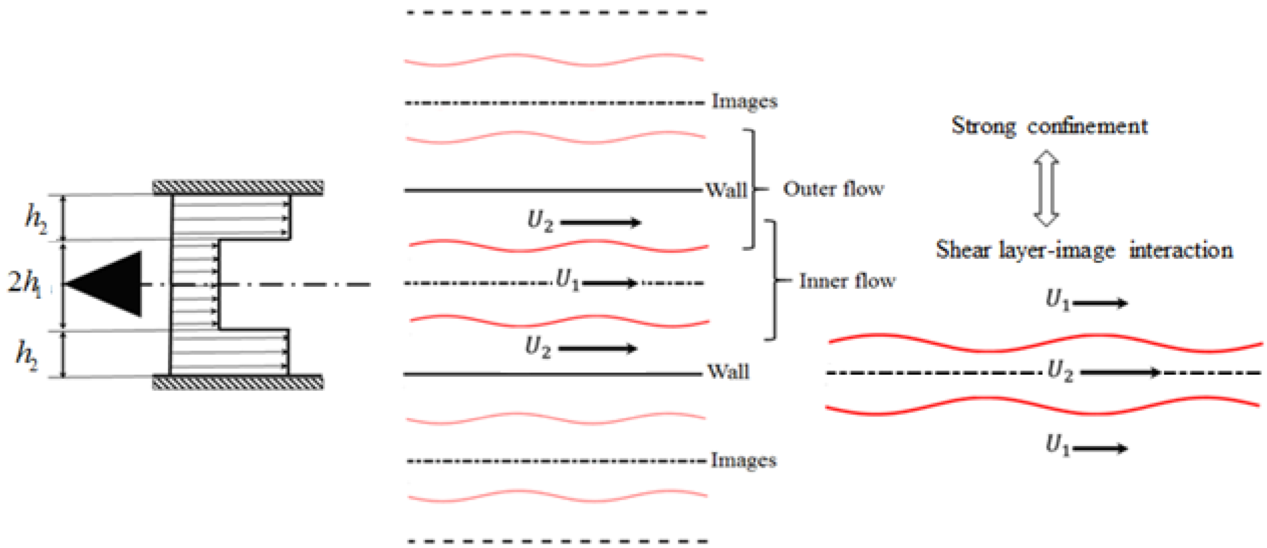

Figure 13. Confined wake system with varicose boundary conditions, illustrating the inner and outer flow regions and the convergence to the outer flow behavior in the strong confinement limit.

The spatio-temporal stability problem is solved for the outer and inner flows independently (i.e. for unconfined jets and wakes) to yield the absolute wave number, k_0 , for each of these flows:

$$k_{0,outer} = -\frac{(1.380 + n\pi)}{h_2} , \tag{15}$$

$$k_{0,inner} = -\frac{(1.380 + m\pi)}{h_1} . \tag{16}$$

In equations 15 and 16, m and n are integers. Values m=0 or n=0 represent the fundamental mode, whereas the higher values denote sub-harmonics. Resonant interaction between the inner and outer flows demands matching of the respective k_0 , which leads to a set of critical L/D.

$$\frac{(1.380 + m\pi)}{h_1} = -\frac{(1.380 + n\pi)}{h_2} . \tag{17}$$

Resonant interaction can occur for fundamental modes or its sub-harmonics and is represented by different values for m and n. For example, m=0 and n=0 denote the interaction between the fundamental modes of the inner and the outer flows. For wakes that are separated by varicose symmetry, these critical values of L/D represent the expected local maxima of $\omega_{0,i}$ as a function of wake spacing.

$$\frac{L}{D} = 1 + \frac{h_2}{h_1} = \frac{(1.380 + n\pi)}{(1.380 + m\pi)} = 2.000, 4.275, 6.550, 8.826 \ \ldots \tag{18}$$

Next, the model is constructed with sinuous wall boundary conditions, which simulates an $n = \infty$ system where the dynamics of each wake is partitioned from those of its neighbors by sinuous symmetry. Following the same methodology yields the critical *L/D* for wakes that are separated by sinuous symmetry.

$$\frac{L}{D} = 1 + \frac{h_2}{h_1} = \frac{(2.950 + n\pi)}{(1.380 + m\pi)} = 3.137, 5.413, 7.688, 9.964 \ \ldots \tag{19}$$

These critical *L/D* values are shown as the dashed vertical lines in Figure 9(a). Comparison of these lines with the confined wake results shows that the RWM result approximately captures the *L*/*D* values with local maxima of $\omega_{0,i}(L/D)$. In addition, it shows that the cases with dominant system-varicose modes are captured by the RWM model in the domain $1.6<L/D<3.2$, $4.1<L/D<5.0$, and so forth. Similarly the RWM predicts the dominant system-sinuous modes in the regime $3.2<L/D<4.1$.

Figure 9(a) shows that, while the model results are close, they do not exactly capture the calculated value of *L/D* at which maximum $\omega_{0,i}$ occurs. Calculations obtained over a range of S-λ (S varying from 0.5 to 6 and $\lambda=-1.0$) combinations, corresponding to both globally stable and unstable conditions, show that the difference is generally less than 5 %.

B. Comparison of stability analysis and experiments

This subsection compares the spatio-temporal stability analysis results on the two-wake system with prior results in the literature. Before making these comparisons, however, several important caveats should be noted: First, for the experimental results, λ, may vary with *L/D* ,while λ values are constant and do not vary with *L/D* for the model problem results shown in the prior section. While it is certainly possible to vary them together, no experimental results have characterized this dependency. Moreover, the experimental velocity profiles are not simple plug flows. Finally, several studies report the presence of asymmetry in the base flow for *L/D* < 1.5, with the gap flow between cylinders biased in one direction or the other [26]. Flow in this case is not parallel. However, at higher Reynolds number and higher spatial separation, the flow approaches the parallel state and the biased gap flow is minimal [51,33]. Thus, the model framework and the base flow profiles provides a realistic representation of the mean flow field over a range of around *L/D* >1.3 and Re > 100 [51]; consequently, we will only consider data in these regimes in this section. However, the fact that λ is not reported in these results implies that the results cannot be directly compared, but qualitative comparisons can be made.

As described in the introduction, experiments show that close interaction of the flow elements is destabilizing, resulting in large scale coherent structures with increased mixing[22, 23, 40]. This is consistent with the destabilizing influence of the additional flow element as predicted by the model stability analysis. For example, Figure 9, comparing the $\omega_{0,i}$ of the n= 2, 3, and 4 systems with that of the unconfined single wake system, reveals that the $\omega_{0,i}$ increases as we increase the number of flow elements, converging onto the dynamics of the $n=\infty$ system for sufficiently large values of *L/D*. These measurements show different symmetry patterns for the vortex shedding, showing system-sinuous behavior at smaller *L/D*, transitioning to system-varicose at larger *L/D*. These theoretical results can be directly compared with that of the variation of the flow patterns observed experimentally as shown in Figure 2. The experiment revealed that the system-sinuous flow pattern occured for smaller *L/D*, as shown in Figure 2 (d), and transitions to the system-varicose structure at larger *L/D*, as shown in Figure 2(a). Moreover, the transition between the two states is intermittent as shown by the Figure 2(b) and (c). This result is consistent with the theory which suggest system-sinuous behavior when *L/D* is closer to one, and transitions to system-varicose as we increase *L/D*. Analogous experimental and numerical studies in the literature also corroborates the observations from the stability analysis [24, 32-34]. Figure 14 summarizes these observations, as well as the predictions of the current study, by plotting the predicted/measured dominant flow pattern as a function of *L/D*. As the experiments do not report a reference shear value, λ, the model results (labeled "current study") show the range in transition values of *L/D* over a physically reasonable range of λ values ($-2.5 < \lambda < -1.0$, based upon looking at the ranges we found in existing literature [13]). Comparing the theory and experimental results, the figure shows that the analysis successfully captures the system-sinuous behavior at small *L/D* and the transition to system varicose at larger *L/D*. Being a linear analysis, it cannot capture the hysteresis behavior, which requires capturing nonlinearities.

The model also predicts that the system will transition from system-varicose to system-sinuous with further increases in *L/D*, as shown in Figure 9. This alternating pattern of system-sinuous and system-varicose dominated modes with increases in *L/D* does not seem to have been experimentally reported. This may be due to the fact that the difference between $\omega_{0,i}$ for the system-sinuous and system-varicose modes becomes increasingly small as *L/D* increases, as both of them have growth rates that asymptote to that of the single, unconfined wake. For example, Figure 6 shows that $\omega_{0,i} D/U_{av}$ at *L/D*=2.0 where the varicose mode is dominant, is -5.24 and -2.32 for the sinuous and varicose modes, a difference of 2.92. In contrast, at *L/D* where the difference between sinuous and varicose again peaks, i.e. at *L/D*=3.2, is only 1.05, and at *L/D*=4.3 it is only 0.37. Thus, the presence of nonlinearity, which the experiments suggest causes one mode to lock in, combined with the progressively decreasing differences in linear growth rates could be responsible for the lack of alteration in dominant flow patterns with *L/D* for the experiments. This result suggests that additional experiments which force a given symmetry (e.g., by initially imposing a sinuous/varicose forcing) and then studying their dominance as a function of *L/D* and forcing history...

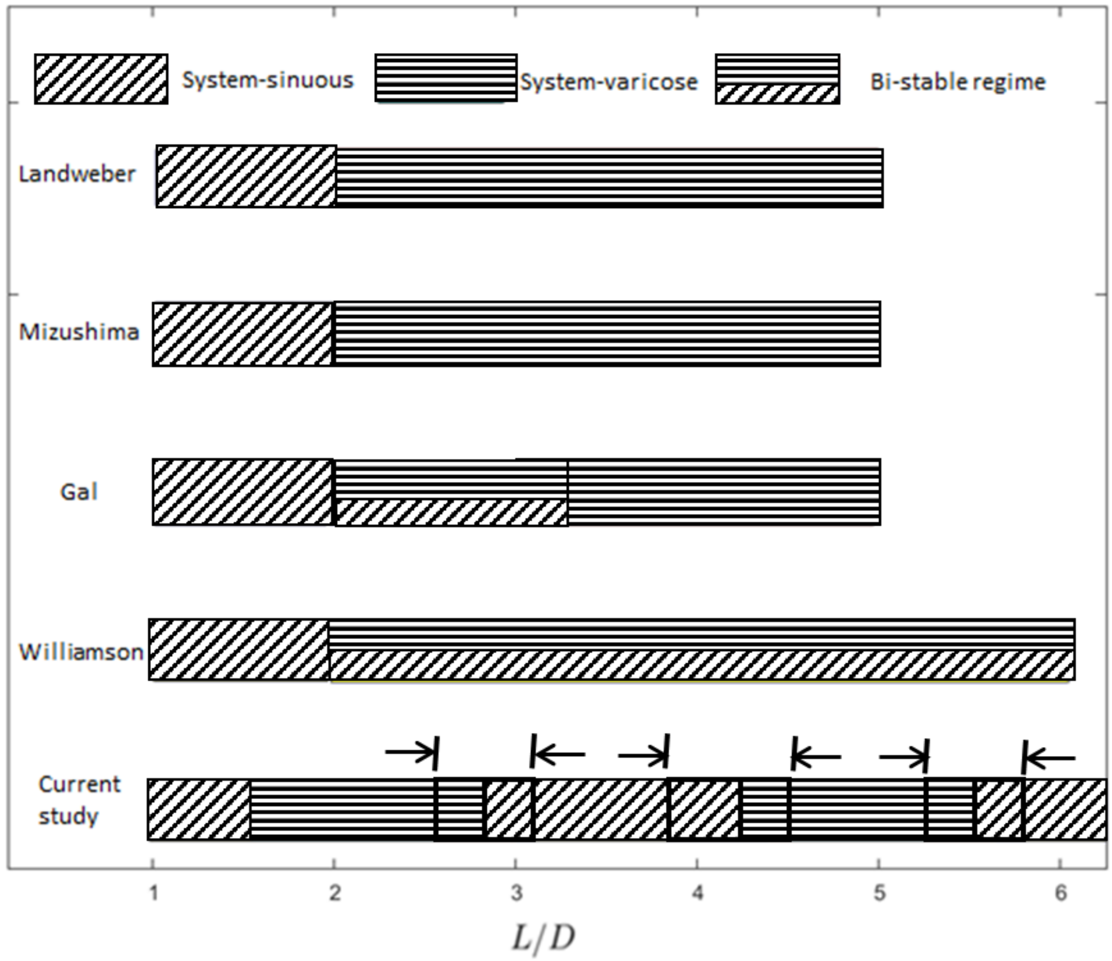

Figure 14: Comparison of the system-sinuous, system-varicose and bi-stable regimes predicted by the analysis presented here (assuming λ=-1.25) and prior experimental and numerical results (Le Gal [33], Williamson[24] ,Mizushima[34] and Landweber [32]). Arrow ranges in "Current Study" shows the variation in the transition *L/D* when λ is varied in the range -1.0 to -2.5.

III. CONCLUSIONS

This paper addresses the question of how the stability characteristics and the resulting flow structure of the multiple wake system differ from those of a single wake system. Key findings from the study are:

(1) *Spatial separation (L/D) effects*: In the limit $L/D \to \infty$, the system limits to the behavior of a single wake. Similarly, in the limit of unity *L/D* (merged wakes) the multi-wake system limits to the behavior of a single wake with diameter equal to *nD*. For intermediate *L/D* values, the $\omega_{0,i}$ of multi-element system varies non-monotonically with spatial separation. This non-monotonic behavior originates from the non-monotonic behavior of the system-sinuous and system-varicose modes, which results in these modes switching dominance as *L/D* is varied. This result explains the experimentally

observed transition for n=2 wake system from a system-sinuous symmetry to that with system-varicose symmetry with increasing L/D[33].

(2) *Effect of the number of elements:* Studies of the dependence of the system behavior for n=2, 3, 4, and ∞ show two L/D regimes where the effects of n are fundamentally different: the near-wake regime where n has a significant influence upon $\omega_{0,i}$, and the far-wake regime where the multi-wake systems converge to a uniform behavior and $\omega_{0,i}$ is only a function of L/D. In general, an increased number of wakes causes destabilization of the most absolutely unstable mode in the multi-wake system (except for L/D~1, where the increasing number of the wakes has a stabilizing influence when the component wakes are absolutely unstable)

(3) *Resonant wave interaction model*[20]: Application of the previously developed resonant wave interaction theory explains why either the system-sinuous or varicose mode dominates at a given L/D value, as well as the L/D value at which $\omega_{0,i}$ peaks. In brief, an inner flow is defined as the central wake feature (a velocity deficit and its neighboring, faster base flow regions) and the the outer flow is defined as a jet that is composed of the faster base flow region, surrounded on one side by the central velocity deficit and on the other side by an image of the velocity deficit. The resonant interaction, when the absolute wave number of the inner flow matches with that of the outer flow, results in the peak destabilization of the multi-wake system.

(4) *Density ratio and shear parameter effects*: In the single wake system, increased density ratio causes a reduction in $\omega_{0,i}$. Similar influence can be brought about by the reduction in the velocity shear ratio. Both the parameters influence the dynamics of the multi-element systems too. Stability boundaries are influenced by both of these parameters. In addition, density ratio and the velocity shear ratio parameter also influences the transition L/D at which the multi-wake system transition from system-sinuous to system-varicose and vice versa.

These results, coupled with prior experiments suggest that further work is needed to characterize the combined effects of nonlinearity. For example, experiments show the presence of hysteresis in L/D value at which the sinuous or varicose mode dominates, something that cannot be assess via a linear analysis Additional nonlinear theory or experiments to further clarify the nature of the bifurcation as a function of L/D would be useful. In addition, the linear theory suggests that the sinuous and varicose mode dominate in an alternating pattern with increasing L/D. While multiple measurements clearly corroborate the first such transition (from sinuous to varicose) with increasing L/D, no successive transitions that the linear theory predicts were experimentally observed. It was suggested that this was due to the progressively decreasing difference in $\omega_{0,i}$ for the sinuous and varicose modes with L/D; the presence of a small nonlinearity could completely suppress this alteration unless the experiment deliberately imposes one symmetry or the other at a given L/D value, such as by adding external forcing.

ACKNOWLEDGMENTS

This research was partially supported by the Air Force Office of Scientific Research (contract #FA9550-16-1-0442), contract monitor Dr. Chiping Li, and the National Science Foundation (Contract No. 1705649), contract monitor, Dr. Song-Charng Kong.

.

REFERENCES

1. S. J. Shanbhogue, S. Husain, and T. Lieuwen, "Lean blowoff of bluff body stabilized flames: Scaling and dynamics," Prog Energ Combust **35**, 98 (2009).

2. T. J. Poinsot, A. C. Trouve, D. P. Veynante, S. M. Candel, and E. J. Esposito, "Vortex-Driven Acoustically Coupled Combustion Instabilities," J Fluid Mech **177**, 265 (1987).

3. B. Emerson, and T. Lieuwen, "Dynamics of harmonically excited, reacting bluff body wakes near the global hydrodynamic stability boundary," J. Fluid Mech. **779**, 716 (2015).

4. A. Prasad, and C. H. Williamson, "The instability of the shear layer separating from a bluff body," Journal of fluid mechanics **333**, 375 (1997).

5. A. E. Perry, M. S. Chong, and T. T. Lim, "The vortex shedding process behind two-dimensional bluff bodies," J. Fluid Mech. **116**, 77 (1982).

6. M. H. Yu, and P. A. Monkewitz, "The effect of nonuniform density on the absolute instability of two-dimensional inertial jets and wakes," Physics of Fluids A: Fluid Dynamics **2**, 1175 (1990).

7. G. Amini, "Linear stability analysis of a liquid jet in a weak crossflow," Phys Fluids **30**, 084105 (2018).

8. J. Deng, L. Sun, L. Teng, D. Pan, and X. Shao, "The correlation between wake transition and propulsive efficiency of a flapping foil: A numerical study," Phys Fluids **28**, 094101 (2016).

9. J. I. Jimenez-Gonzalez, and P. Brancher, "Transient energy growth of optimal streaks in parallel round jets," Phys Fluids **29**, 114101 (2017).

10. G. Ogus, M. Baelmans, and M. Vanierschot, "On the flow structures and hysteresis of laminar swirling jets," Phys Fluids **28**, 123604 (2016).

11. T. Radko, and D. Lorfeld, "Effects of weak planetary rotation on the stability and dynamics of internal stratified jets," Phys Fluids **30**, 096602 (2018).

12. R. Erickson, and M. Soteriou, "The influence of reactant temperature on the dynamics of bluff body stabilized premixed flames," Combustion and Flame **158**, 2441 (2011).

13. B. Emerson, J. O'Connor, M. Juniper, and T. Lieuwen, "Density ratio effects on reacting bluff-body flow field characteristics," Journal of Fluid Mechanics **706**, 219 (2012).

14. B. L. Emerson, D. R. Noble, and T. C. Lieuwen, "Stability Analysis of Reacting Wakes: The Physical Role of Flame-Shear Layer Offset" (2014).

15. K. Sreenivasan, S. Raghu, and D. Kyle, "Absolute instability in variable density round jets," Experiments in Fluids **7**, 309 (1989).

16. S. Ravier, M. Abid, M. Amielh, and F. Anselmet, "Direct numerical simulations of variable-density plane jets," J Fluid Mech **546**, 153 (2006).
17. M. Roa, and D. G. Talley, "Vortex Dynamic Mechanisms in Coaxial Hydrogen/LOX Jet Flames" (2018).
18. M. Roa, D. Forliti, A. Badakhsahn, and D. Talley, "Acoustically Forced Coaxial Hydrogen/Liquid Oxygen Jet Flames", Document No. Number, 2016.
19. M. P. Juniper, and S. M. Candel, "The stability of ducted compound flows and consequences for the geometry of coaxial injectors," J Fluid Mech **482**, 257 (2003).
20. M. P. Juniper, "The effect of confinement on the stability of two-dimensional shear flows," J Fluid Mech **565**, 171 (2006).
21. M. Zdravkovich, "Review of flow interference between two circular cylinders in various arrangements," Journal of Fluids Engineering **99**, 618 (1977).
22. P. Bearman, and A. Wadcock, "The interaction between a pair of circular cylinders normal to a stream," J Fluid Mech **61**, 499 (1973).
23. S. Ishigai, E. Nishikawa, K. Nishimura, and K. Cho, "Experimental study on structure of gas flow in tube banks with tube axes normal to flow: Part 1, Karman vortex flow from two tubes at various spacings," Bulletin of JSME **15**, 949 (1972).
24. C. Williamson, "Evolution of a single wake behind a pair of bluff bodies," J Fluid Mech **159**, 1 (1985).
25. E.-i. Hori, "Experiments on flow around a pair of parallel circular cylinders" (1959).
26. D. Sumner, S. Wong, S. Price, and M. Paidoussis, "Fluid behaviour of side-by-side circular cylinders in steady cross-flow," Journal of Fluids and Structures **13**, 309 (1999).
27. H.-J. Kim, and P. Durbin, "Investigation of the flow between a pair of circular cylinders in the flopping regime," Journal of Fluid Mechanics **196**, 431 (1988).
28. M. Carini, F. Giannetti, and F. Auteri, "On the origin of the flip–flop instability of two side-by-side cylinder wakes," Journal of Fluid Mechanics **742**, 552 (2014).
29. Z. Wang, and Y. Zhou, "Vortex interactions in a two side-by-side cylinder near-wake," International journal of heat and fluid flow **26**, 362 (2005).
30. H. M. Spivack, "Vortex frequency and flow pattern in the wake of two parallel cylinders at varied spacing normal to an airstream," Catholic University of America, 1945.
31. B. Cantwell, and D. Coles, "An experimental study of entrainment and transport in the turbulent near wake of a circular cylinder," Journal of fluid mechanics **136**, 321 (1983).
32. L. Landweber, "Flow about a pair of adjacent, parallel cylinders normal to stream- theoretical analysis", Document No. Number, 1942.
33. I. Peschard, and P. Le Gal, "Coupled wakes of cylinders," Phys Rev Lett **77**, 3122 (1996).
34. J. Mizushima, and T. Akinaga, "Vortex shedding from a row of square bars," Fluid Dyn Res **32**, 179 (2003).
35. S. Kang, "Characteristics of flow over two circular cylinders in a side-by-side arrangement at low Reynolds numbers," Phys Fluids **15**, 2486 (2003).
36. M. Meehan, A. Tyagi, and J. O'Connor, "Flow dynamics in a variable-spacing, three bluff-body flowfield," Phys Fluids **30**, 025105 (2018).
37. Q. Zheng, and M. M. Alam, "Intrinsic features of flow past three square prisms in side-by-side arrangement," J Fluid Mech **826**, 996 (2017).

38. P. Le Gal, I. Peschard, M. Chauve, and Y. Takeda, "Collective behavior of wakes downstream a row of cylinders," Phys Fluids **8**, 2097 (1996).
39. D. R. Miller, and E. W. Comings, "Force-momentum fields in a dual-jet flow," Journal of Fluid Mechanics **7**, 237 (1960).
40. E. A. Anderson, D. O. Snyder, and J. Christensen, "Periodic flow between low aspect ratio parallel jets," Journal of fluids engineering **125**, 389 (2003).
41. H. Sato, "The stability and transition of a two-dimensional jet," Journal of Fluid Mechanics **7**, 53 (1960).
42. N. E. Bunderson, and B. L. Smith, "Passive mixing control of plane parallel jets," Experiments in Fluids **39**, 66 (2005).
43. C. Soong, P. Tzeng, and C. Hsieh, "Numerical investigation of flow structure and bifurcation phenomena of confined plane twin-jet flows," Phys Fluids **10**, 2910 (1998).
44. G. Schweiger, "Regular structures in a plane triple jet," Journal of Fluids Engineering **105**, 42 (1983).
45. B. Emerson, S. Jagtap, J. M. Quinlan, M. W. Renfro, B. M. Cetegen, and T. Lieuwen, "Spatio-temporal linear stability analysis of stratified planar wakes: Velocity and density asymmetry effects. ," Physics of Fluids (1994-present) **28**, (2016).
46. S. J. Rees, "Hydrodynamic instability of confined jets & wakes & implications for gas turbine fuel injectors," University of Cambridge, 2010.
47. R. J. Briggs, "Electron-stream interaction with plasmas," (1964).
48. H. Bénard, "H. Bénard, CR Hebd. Seances Acad. Sci. 147, 839 (1908)," CR Hebd. Seances Acad. Sci. **147**, 839 (1908).
49. T. Von Kármán, "Über den Mechanismus des Widerstandes, den ein bewegter Körper in einer Flüssigkeit erfährt," Nachrichten von der Gesellschaft der Wissenschaften zu Göttingen, Mathematisch-Physikalische Klasse **1911**, 509 (1911).
50. T. V. Karman, "Über den Mechanismus des Wiederstandes, den ein bewegter Korper in einer Flüssigkeit erfahrt," Nachrichten von der Gesellschaft der Wissenschaften zu Göttingen, Mathematisch-Physikalische Klasse **1912**, 547 (1912).
51. S. Xu, Y. Zhou, and R. So, "Reynolds number effects on the flow structure behind two side-by-side cylinders," Physics of Fluids **15**, 1214 (2003).